Nitridation of Al_2O_3 Surfaces: Chemical and Structural Change Triggered by Oxygen Desorption

Toru Akiyama,* Yasutaka Saito, Kohji Nakamura, and Tomonori Ito
Department of Physics Engineering, Mie University, 1577 Kurima-Machiya, Tsu 514-8507, Japan
(Received 5 August 2012; published 7 January 2013)

We present theoretical investigations that clarify elemental nitridation processes of corundum $Al_2O_3(0001)$ and $(1\bar{1}02)$ surfaces. The calculations within the density functional theory framework reveal that the structures with substitutional N atoms beneath the surface are stabilized under nitridation conditions. We also find that the desorption of O atoms at the topmost layer induces outward diffusion of O atoms as well as inward diffusion of N atoms, leading to the transformation into AlN films. The kinetic Monte Carlo simulations in conjunction with density functional theory results indeed observe a dependence of these chemical and structural changes on temperature and pressure.

DOI: 10.1103/PhysRevLett.110.026101 PACS numbers: 68.43.Mn, 68.43.Bc, 81.65.−b, 82.20.Wt

The nature of metal oxide surfaces is quite important in various technological applications. In particular, corundum Al_2O_3 surfaces are employed as substrates for epitaxial growth of other materials. Nitride semiconductors such as GaN and AlN are epitaxially grown on an Al_2O_3 substrate [1,2] and recently carbon nanotubes have been aligned along the direction of its certain surfaces [3,4]. Microscopic identification of atomic and electronic structures of Al_2O_3 surfaces is thus imperative at various stages in current technology and the understanding of its physics and chemistry is of great importance.

The exposure of Al_2O_3 surfaces to ammonia and N radicals with high temperatures ($\sim$1400 K) is usually performed to improve structural and luminescent properties of epitaxial GaN films, and is now one of the essential techniques for the fabrication of high-quality GaN and AlN films on Al_2O_3 substrates [5–8]. Previous experimental studies have reported that these improvements result from the formation of buffer AlN layers by nitridation on Al_2O_3 surfaces [9–19]. The analysis of nitrided layers on an $Al_2O_3(0001)$ surface by means of high-energy electron diffraction, x-ray photoelectron spectroscopy (XPS), and transmission electron microscopy has proposed the formation of relaxed crystalline AlN [11–15,19] while several studies have shown the formation of amorphous aluminum oxynitride layers [10,16–18]. More recently, the nitridation on an $Al_2O_3(1\bar{1}02)$ surface has been found to improve the crystal quality and surface morphology of expitaxial GaN grown along nonpolar $(11\bar{2}0)$ orientation [20,21]. Despite these experimental efforts, the atomic-scale understanding of chemical and structural change caused by nitrogen on Al_2O_3 surfaces is still unclear.

In contrast, previous theoretical investigations on the surface in metal-oxide materials such as Al_2O_3 were mainly focused on surface stoichiometries and structures under realistic conditions [22–25]. The structures and properties have been found to change drastically depending upon the chemical potential of gas-phase species in equilibrium with the surface at different temperatures [23,24]. Yet, to our knowledge, interactions of nitrogen with Al_2O_3 surfaces with a realistic environment have not been investigated in theoretical studies. There are still open questions of how nitrided films with different stoichiometry compared with Al_2O_3 are formed during the nitridation.

In this Letter, we theoretically investigate nitridation processes of Al_2O_3 surfaces taking account of realistic conditions such as temperature and pressure of gas-phase species. Our surface energy calculations at given temperature and pressure within the density functional theory (DFT) framework [26] clarify that nitrogen incorporated surfaces with oxygen desorption are stabilized under nitridation conditions. On the basis of DFT calculations, we also perform kinetic Monte Carlo (KMC) simulations and find that the outward diffusion of oxygen induced by oxygen desorption is crucial for the formation of AlN layers.

Here, we focus on technologically important $Al_2O_3(0001)$ and $(1\bar{1}02)$ substrates on which nitride semiconductors are epitaxially grown with polar and nonpolar orientations, respectively. The slab model consisting of six oxygen layers and 12 aluminum layers is adopted for $Al_2O_3(0001)$ surface, whereas that of 12 oxygen layers and eight aluminum layers is used for $Al_2O_3(1\bar{1}02)$ surface. Configurations are labeled as $n_N n_O n_{Al} x$, where n_N, n_O, and n_{Al} are the numbers of additional N, O, and Al atoms with respect to the reference surface, respectively. As a reference surface, we use the stoichiometric Al-terminated and O-terminated surface structures for (0001) and $(1\bar{1}02)$ orientations, respectively [24,25]. The letter x specifies the different configurations with the same n_i, and the configurations are labeled simply as $n_N/n_O x$ when n_{Al} is zero. The stability of surfaces with different stoichiometries in equilibrium with the gas phase is determined by the surface energy $E_{surf}(n_N/n_O/n_{Al}x)$ as functions of chemical potentials. The surface energy at temperature T and pressure p_i of the ith type of atoms is given by $E_{surf}(n_N/n_O/n_{Al}x) = E_{tot}(n_N/n_O/n_{Al}x) - E_{ref} - \sum n_i \mu_i(p_i, T)$, where $E_{tot}(n_N/n_O/n_{Al}x)$ and E_{ref} are the total energy of the surface under consideration and of the reference surface obtained by DFT calculations as shown in

 © 2013 American Physical Society

Sec. 1.1 of Ref. [27]. n_i is the number of excess ith-type atoms with respect to the reference and $\mu_i(p_i, T)$ is the chemical potential at given temperature and pressure [28,29]. Here, we assume that the chemical potential of Al is in equilibrium with bulk Al_2O_3. The nudged elastic band method is used to obtain the energy barrier of each elemental process, such as substitution and diffusion [30]. On the basis of these DFT calculation results, KMC simulations are performed to infer the nitridation processes and resultant atomic arrangement under nitridation conditions. In our KMC calculations, adsorption, desorption, substitution, and diffusion of constituent elements are evaluated in each MC step. Details of the KMC calculation procedure are described in Sec. 1.2 of Ref. [27].

Our DFT calculations for more than 100 configurations indeed elucidate that the stable structures dramatically change depending on temperature and pressures. The desorption of oxygen does not occur and the surfaces with N adatoms are stabilized at 0 K (Fig. S1 of Ref. [27]), whereas N atoms are substituted for O atoms located beneath the surface under high temperature conditions [31]. Figure 1 shows the calculated surface energy under typical nitridation conditions ($T = 1400$ K, $p_N = 1 \times 10^{-4}$ Torr, and $p_{O_2} = 1 \times 10^{-8}$ Torr) as a function of total number of atoms $N_{at} = \sum |n_i|$, which corresponds to the number of elemental processes during nitridation. The surface energy decreases with the number of atoms and takes the lowest value for $N_{at} = 8$ ($3/\text{-}5a$) and $N_{at} = 5$ ($2/\text{-}3a$) on (0001) and $(1\bar{1}02)$ orientations, respectively. The negative values of E_{surf} for large N_{at} indicate that structural changes toward the stable structures from the initial stoichiometric surfaces $[E_{surf}(0/0a) = 0$ eV$]$ proceed under nitridation conditions.

For both orientations, these stable surfaces no longer maintain the stoichiometry of Al_2O_3. As shown in the inset of Fig. 1(a), three N atoms are substituted for O atoms and in total five O atoms desorb from the surface on (0001) orientation. In the case of $(1\bar{1}02)$ orientation shown in Fig. 1(b), two N atoms are substituted for O atoms and in total three O atoms desorb from the surface. Considering the stoichiometry of AlN and Al_2O_3, the incorporation of two N atoms and desorption of three O atoms is at least required for AlN formation. Since these stable surfaces satisfy this condition and all the O atoms in the second anion layer are completely replaced by N atoms, they can be regarded as AlN layers generated by one monolayer (ML) of Al_2O_3. At the interface between resultant AlN layer and the substrate, an important structural feature is also recognized. As shown in the insets of Fig. 1, the stable structures $3/\text{-}5a$ and $2/\text{-}3a$ on (0001) and $(1\bar{1}02)$ orientations satisfy the in-plane alignment written as AlN$[10\bar{1}0] \parallel Al_2O_3[11\bar{2}0]$ and AlN$[0001] \parallel Al_2O_3[\bar{1}101]$, respectively. If we assume that nitride semiconductors are epitaxially grown on these stable structures, the in-plane alignments between nitrides and the substrate satisfy $[10\bar{1}0]_{nitrides} \parallel [11\bar{2}0]_{sapphire}$ and $[0001]_{nitrides} \parallel [\bar{1}101]_{sapphire}$ for (0001) and $(1\bar{1}02)$ orientations, respectively. These alignments agree well with those obtained by reflection high-energy electron diffraction [9,19,32,33] and transmission electron microscopy [13,15] observations, supporting that the formation of AlN layers leads to the improvement of structural and optical properties of nitrides after the nitridation.

Another important feature of E_{surf} in Fig. 1 is related to the most stable configuration for each n_N/n_O with N atoms. The most stable configurations labeled as n_N/n_Oa in Fig. 1 contain substitutional N atoms beneath the surface. On the other hand, the energy of the surface with N atoms (labeled n_N/n_Ob) at the topmost layer are ~1.32 eV

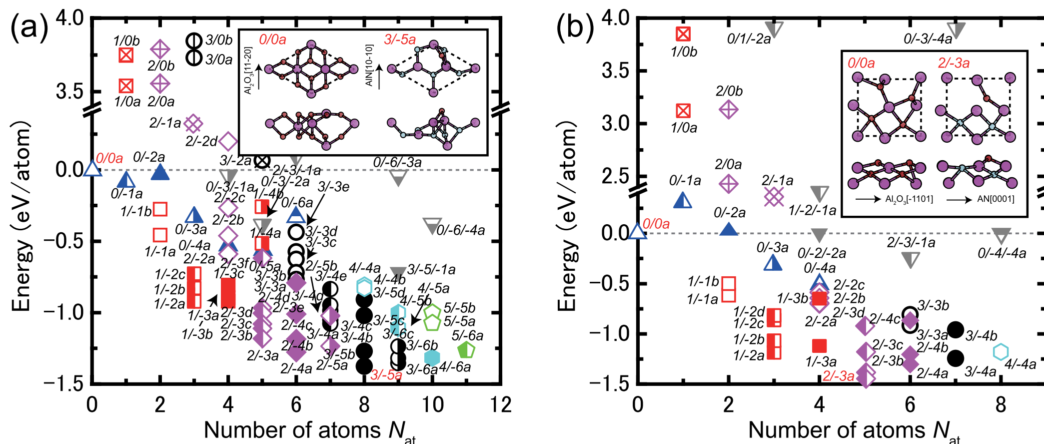

FIG. 1 (color online). Calculated surface energy of (a) $Al_2O_3(0001)$ and (b) $Al_2O_3(1\bar{1}02)$ surfaces as a function of total number of adsorption and desorption atoms $N_{at} = \sum |n_i|$. Only data for $-1.5 \le E_{surf} \le 4.0$ eV are displayed. Triangles correspond to the surfaces without N atoms, and squares, diamonds, circles, hexagons, and pentagons to the surfaces with one, two, three, four, and five nitrogen atoms in the unit cell, respectively. The surfaces with Al desorption are represented by inverted triangles. Patterns of symbols are defined by the difference between the number of incorporated N atoms and that of desorbing O atoms. Insets represent top and side views of stable surfaces with N atoms ($3/\text{-}5a$ and $2/\text{-}3a$ on (0001) and $(1\bar{1}20)$ surfaces, respectively) and without N atom ($0/0a$), along with the in-plane directions. Large and filled (empty) small circles represent Al and O (N) atoms, respectively.

higher than that with N atoms beneath the surface. The surfaces with a substitutional N atom at the topmost layer are therefore metastable. The stabilization of a N incorporated surface is due to the formation of amphoteric (both covalent and ionic) Al-N bonds, whose bond energy is larger than that of Al-O bonds. The number of Al-N bonds in the substitutional N atom beneath the surface is larger than that in the N atom at the topmost layer. Therefore, the stabilization of N atoms beneath the surface is a driving force toward the formation of AlN layers, and structural changes such as rearrangement of O and N atoms as well as oxygen desorption and nitrogen adsorption are substantial processes during the nitridation.

The inspection of structural change indeed demonstrates several elemental processes leading to the rearrangements of O and N atoms. Table I summarizes each elemental process, its reaction energy E_r, and energy barrier E_b obtained by the nudged elastic band method (Sec. 3 in Ref. [27]). The energy barrier for the concerted exchange [34] between the N atom located at the topmost layer and the O atom beneath the surface ($1/\text{-}1b \rightarrow 1/\text{-}1a$) takes a quite large value [$E_b = 5.73$ and 5.70 eV on (0001) and $(1\bar{1}02)$ surfaces, respectively] compared with that of other elemental processes. The concerted exchange is thus virtually negligible and hardly involved in the incorporation of N atoms into the surfaces. In contrast, E_r takes a positive value and E_b is small for nitrogen indiffusion for $\Delta n = n_{\mathrm{O}} + n_{\mathrm{N}} \leq -1$. This suggests that the indiffusion of N atoms and the formation of substitutional N atoms beneath the surface occur when metastable structures (labeled $n_{\mathrm{N}}/n_{\mathrm{O}}c$ or $n_{\mathrm{N}}/n_{\mathrm{O}}e$) caused by oxygen outward diffusion are formed. The high-energy barrier for oxygen outdiffusion compared with that for nitrogen indiffusion suggests that the outward diffusion of oxygen rather than inward diffusion of nitrogen is expected to be a dominant elemental process.

The difference in the energy barrier depending on diffusion species can be attributed to the number of amphoteric bonds. This is exemplified in $3/\text{-}5b$ on an $Al_2O_3(0001)$ surface shown in Fig. 2. The positive values in the charge density difference between the O atom and its neighboring Al atoms for $3/\text{-}5b$ on an $Al_2O_3(0001)$ surface shown in Fig. 2(a) exhibit the formation of four Al-O bonds. On the contrary, there are few charge density differences between the O atom and two of the neighboring Al atoms (labeled Al1 and Al2) in the transition state structure shown in Fig. 2(b). Accordingly, the interatomic distances between O and Al atoms [from 1.92 (2.10) to

TABLE I. Elemental process during structural change into AlN on Al_2O_3 surfaces. Initial and final states, reaction energy E_r (energy difference between initial and final states), energy barrier E_b obtained by the nudged elastic band method, and type of elemental process are listed. Positive (negative) values in E_r correspond to exothermic (endothermic) reactions. D_{N}, D_{O}, and C_{NO} denote indiffusion of N atom, outdiffusion of O atom, and concerted exchange between N and O atoms, respectively. Geometries and energy profiles are depicted in Fig. S3 of Ref. [27].

Orientation	Structures	E_r (eV)	E_b (eV)	Process type
(0001)	$1/\text{-}1b \rightarrow 1/\text{-}1a$	0.37	5.73	C_{NO}
	$1/\text{-}2b \rightarrow 1/\text{-}2c$	−0.61	1.15	D_{O}
	$1/\text{-}2c \rightarrow 1/\text{-}2a$	1.15	0.20	D_{N}
	$1/\text{-}3b \rightarrow 1/\text{-}3c$	−1.01	1.62	D_{O}
	$1/\text{-}3c \rightarrow 1/\text{-}3a$	1.17	0.12	D_{N}
	$2/\text{-}3d \rightarrow 2/\text{-}3e$	−0.10	1.29	D_{O}
	$2/\text{-}3e \rightarrow 2/\text{-}3b$	1.89	0.47	D_{N}
	$2/\text{-}3b \rightarrow 2/\text{-}3c$	−0.11	1.21	D_{O}
	$2/\text{-}3c \rightarrow 2/\text{-}3a$	0.43	0.89	D_{N}
	$2/\text{-}4b \rightarrow 2/\text{-}4c$	−0.90	0.91	D_{O}
	$2/\text{-}4c \rightarrow 2/\text{-}4a$	1.79	0.26	D_{N}
	$3/\text{-}4d \rightarrow 3/\text{-}4e$	−0.99	1.30	D_{O}
	$3/\text{-}4e \rightarrow 3/\text{-}4b$	1.35	0.44	D_{N}
	$3/\text{-}4b \rightarrow 3/\text{-}4c$	−0.11	2.33	D_{O}
	$3/\text{-}4c \rightarrow 3/\text{-}4a$	1.00	0.53	D_{N}
	$3/\text{-}5b \rightarrow 3/\text{-}5c$	−1.45	2.83	D_{O}
	$3/\text{-}5c \rightarrow 3/\text{-}5a$	2.28	1.14	D_{N}
$(1\bar{1}02)$	$1/\text{-}1b \rightarrow 1/\text{-}1a$	0.23	5.70	C_{NO}
	$1/\text{-}2b \rightarrow 1/\text{-}2c$	−0.78	1.03	D_{O}
	$1/\text{-}2c \rightarrow 1/\text{-}2a$	1.32	0.85	D_{N}
	$2/\text{-}3b \rightarrow 2/\text{-}3c$	−1.49	1.79	D_{O}
	$2/\text{-}3c \rightarrow 2/\text{-}3a$	1.15	0.11	D_{N}

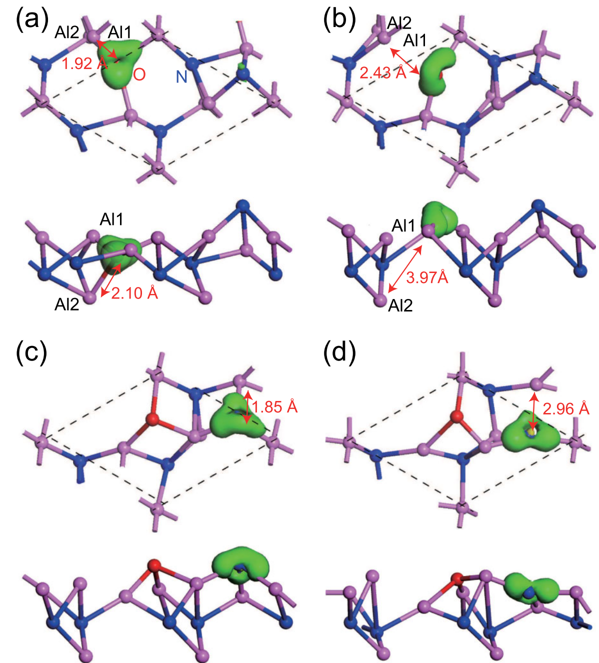

FIG. 2 (color online). Top and side views of charge density difference between the surface with diffusing atom and a simple sum of the surface without diffusing atom and O/N atom for (a) N atom at the topmost layer $3/\text{-}5b$, (b) transition state structure for oxygen outdiffusion, (c) N and O atoms at topmost layer $3/\text{-}5c$, and (d) transition state structure for nitrogen indiffusion on $Al_2O_3(0001)$ surface. Positive (accumulated) and negative (depleted) values are represented by green and yellow regions, respectively. Isosurfaces are ± 0.01 electron/Å^3. Interatomic distances (in Å) are also shown.

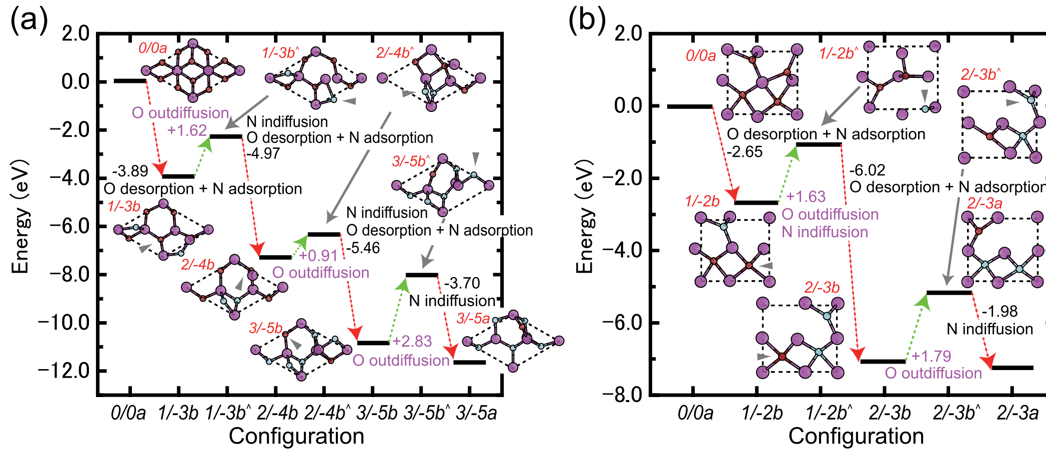

FIG. 3 (color online). Geometries and energy profiles (in eV) of (a) $Al_2O_3(0001)$ and (b) $Al_2O_3(1\bar{1}02)$ surfaces during nitridation processes obtained by KMC simulations under typical nitridation conditions ($T = 1400$ K, $p_N = 1 \times 10^{-4}$ Torr, and $p_{O_2} = 1 \times 10^{-8}$ Torr). The notation of atoms is the same as in Fig. 1. We add ∧ to each configuration for transition state structures in O/N diffusion (for instance, $n_N/n_O x^\wedge$). Arrowheads indicate diffusing N and O atoms. Note that the atomic coordinates in the figure are obtained by DFT calculations.

2.43 (3.97) Å for O-Al1 (O-Al2)] are drastically elongated in the transition state, supporting the dissociation of Al-O bonds. These features can also be seen during nitrogen indiffusion shown in Figs. 2(c) and 2(d), but only one Al-N bond dissociates during the indiffusion.

Figure 3 shows geometries and energy profiles during nitridation processes obtained by KMC simulations on the basis of rates derived from DFT calculations. Although various types of elemental processes are incorporated in the KMC simulations, the nitridation consists of a sequence of four types of elemental processes. For both orientations, N atoms adsorb on the topmost layer after the desorption of O atoms. The outdiffusion of oxygen located beneath the surface and indiffusion of the N atom (arrowheads in Fig. 3) proceed after the nitrogen adsorption. This set of elemental processes repeats until 1 ML of an AlN layer is formed. Since the energy barriers for oxygen outdiffusion are higher than those of nitrogen indiffusion, the stable structures with N atoms beneath the surface cannot be generated without the outdiffusion of O atoms. It is thus concluded that, irrespective of surface orientation, outward diffusion of O atoms located beneath the surface is a rate-limiting factor.

Indeed, KMC simulations for various temperatures provide a consequence of oxygen diffusion. Figure 4 shows the rate for AlN formation as a function of reciprocal temperature estimated from KMC calculations. Here, the rate is defined as the reciprocal of time for AlN formation. The time for AlN formation is calculated by an integral of time increments until the formation of 1 ML of an AlN layer. Owing to an enhancement of oxygen diffusion at high temperatures, the rate increases monotonically with temperature. This trend is qualitatively consistent with the temperature dependence of XPS intensity corresponding to Al-N bonds [14].

Furthermore, several important features which can be compared with the experiments can be deduced from the rate shown in Fig. 4. At each temperature the rate with high nitrogen pressure is larger than that with low pressure, indicating that the rate increases with nitrogen pressure. The pressure dependence results from high adsorption probability of N atoms under high nitrogen pressure conditions, and reasonably agrees with that in XPS intensity [14,19]. Furthermore, the rate on an $Al_2O_3(1\bar{1}02)$ surface is found to be always higher than that on an $Al_2O_3(0001)$ surface. The orientation dependence implies that the

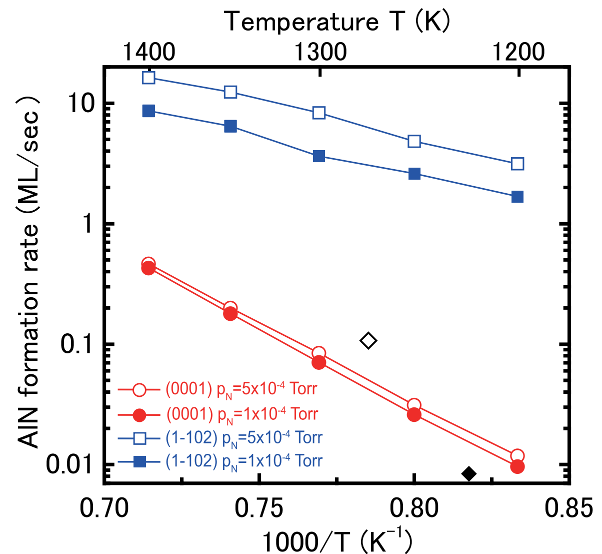

FIG. 4 (color online). Calculated nitridation rate on Al_2O_3 surfaces as a function of reciprocal temperature obtained by KMC simulations. Circles and squares represent the growth rate on $Al_2O_3(0001)$ and $(1\bar{1}02)$ surfaces, respectively. Filled and empty symbols denote the results with nitrogen pressures at $p_N = 1 \times 10^{-4}$ and 5×10^{-4} Torr, respectively. Experimental data for $Al_2O_3(0001)$ [13] and $(1\bar{1}02)$ [9] surfaces are shown as filled and empty diamonds, respectively.

nitridation on nonpolar orientation is faster than that on polar (0001) orientation. This is because the energy barrier for oxygen outdiffusion in $3/\text{-}5b$ on an $Al_2O_3(0001)$ surface (2.83 eV) is higher than that in $2/\text{-}3b$ on an $Al_2O_3(1\bar{1}02)$ surface (1.79 eV) due to the dissociation of two Al-O bonds. The overestimation of the calculated formation rate compared with the experiments might be due to the diffusion of N and O atoms in AlN layers with more than 2 MLs, which are not taken into account in our KMC simulations. Since these diffusion processes are expected to be insensitive to surface orientation, the formation rate is still dependent on oxygen outdiffusion, and the rate on nonpolar orientation could be faster than that on polar (0001) orientation even for AlN layers with more than 2 MLs. This trend is reasonably consistent with experimentally reported growth rate difference (diamonds in Fig. 4) [9,13]. Clarifying further elemental processes such as diffusion of O and N atoms in AlN layers during nitridation should be desirable to predict the formation rate of AlN layers more quantitatively.

In summary, on the basis of DFT calculations we have proposed a novel mechanism in which the desorption of O atoms at the topmost layer induces oxygen outdiffusion as well as nitrogen induffusion. As a result of these elemental processes, transformation into AlN layers occurs under nitridation conditions. The KMC simulations on the basis of rates derived from DFT calculations identify the growth rate difference of AlN layers depending on surface orientation, consistent with experimental results.

This work was supported in part by Grant-in-Aid for Scientific Research (No. 24560025) from the JSPS. Computations were performed at RCCS (National Institutes of Natural Sciences).

*akiyama@phen.mie-u.ac.jp

[1] H. Amano, N. Sawaki, I. Akasaki, and Y. Toyoda, Appl. Phys. Lett. **48**, 353 (1986).
[2] S. Nakamura, Y. Harada, and M. Seno, Appl. Phys. Lett. **58**, 2021 (1991).
[3] S. Han, X. Liu, and C. Zhou, J. Am. Chem. Soc. **127**, 5294 (2005).
[4] N. Ishigami, H. Ago, K. Imamoto, M. Tsuji, K. Iakoubovskii, and N. Minami, J. Am. Chem. Soc. **130**, 9918 (2008).
[5] S. Keller, B. P. Keller, Y.-F. Wu, B. Heying, D. Kapolnek, J. S. Speck, U. K. Mishra, and S. P. DenBaars, Appl. Phys. Lett. **68**, 1525 (1996).
[6] N. Grandjean, J. Massies, and M. Leroux, Appl. Phys. Lett. **69**, 2071 (1996).
[7] M. H. Kim, C. Sone, J. H. Yi, and E. Yoon, Appl. Phys. Lett. **71**, 1228 (1997).
[8] F. Widmann, G. Feuillet, B. Daudin, and J. L. Rouvière, J. Appl. Phys. **85**, 1550 (1999).
[9] K. Masu, Y. Nakamura, T. Yamazaki, and T. S. T. Tsubouchi, Jpn. J. Appl. Phys. **34**, L760 (1995).
[10] K. Uchida, A. Watanabe, F. Yano, M. Kouguchi, T. Tanaka, and S. Minagawa, J. Appl. Phys. **79**, 3487 (1996).
[11] N. Grandjean, J. Massies, Y. Martinez, P. Venngues, M. Leroux, and M. Lagt, J. Cryst. Growth **178**, 220 (1997).
[12] M. Seelmann-Eggebert, H. Zimmermann, H. Obloh, R. Niebuhr, and B. Wachtendorf, J. Vac. Sci. Technol. A **16**, 2008 (1998).
[13] M. Yeadon, M. T. Marshall, F. Hamdani, S. Pekin, H. Morkoç, and J. M. Gibson, J. Appl. Phys. **83**, 2847 (1998).
[14] T. Hashimoto, Y. Terakoshi, M. Ishida, M. Yuri, O. Imafuji, T. Sugino, A. Yoshikawa, and K. Itoh, J. Cryst. Growth **189–190**, 254 (1998).
[15] Y. Cho, Y. Kim, E. R. Weber, S. Ruvimov, and Z. Liliental-Weber, J. Appl. Phys. **85**, 7909 (1999).
[16] T. Hashimoto, Y. Terakoshi, M. Yuri, M. Ishida, O. Imafuji, T. Sugino, and K. Itoh, J. Appl. Phys. **86**, 3670 (1999).
[17] M. Losurdo, P. Capezzuto, and G. Bruno, J. Appl. Phys. **88**, 2138 (2000).
[18] G. Namkoong, W. A. Doolittle, A. S. Brown, M. Losurdo, P. Capezzuto, and G. Bruno, J. Appl. Phys. **91**, 2499 (2002).
[19] F. Dwikusuma and T. F. Kuech, J. Appl. Phys. **94**, 5656 (2003).
[20] J.-J. Wu, Y. Katagiri, K. Okuura, D.-B. Li, H. Miyake, and K. Hiramatsu, J. Cryst. Growth **311**, 3801 (2009).
[21] B. Ma, W. Hu, H. Miyake, and K. Hiramatsu, Appl. Phys. Lett. **95**, 121910 (2009).
[22] V. Puchin, J. Gale, A. Shluger, E. Kotomin, J. Günster, M. Brause, and V. Kempter, Surf. Sci. **370**, 190 (1997).
[23] R. DiFelice and J. E. Northrup, Phys. Rev. B **60**, R16287 (1999).
[24] X.-G. Wang, A. Chaka, and M. Scheffler, Phys. Rev. Lett. **84**, 3650 (2000).
[25] T. Kurita, K. Uchida, and A. Oshiyama, Phys. Rev. B **82**, 155319 (2010).
[26] M. Tsukada *et al.*, Computer Program Package TAPP (University of Tokyo, Tokyo, Japan, unpublished); J. Yamauchi, M. Tsukada, S. Watanabe, and O. Sugino, Phys. Rev. B **54**, 5586 (1996); H. Kageshima and K. Shiraishi, Phys. Rev. B **56**, 14985 (1997).
[27] See Supplemental Material at http://link.aps.org/supplemental/10.1103/PhysRevLett.110.026101 for detailed descriptions of DFT calculations and the KMC method. Furthermore, it includes figures of E_{surf} at 0 K, detailed geometries and energy profiles for each elemental process, and details of structural change obtained by KMC simulations.
[28] Y. Kangawa, T. Ito, A. Taguchi, K. Shiraishi, and T. Ohachi, Surf. Sci. **493**, 178 (2001).
[29] Y. Kangawa, T. Ito, A. Taguchi, K. Shiraishi, T. Irisawa, and T. Ohachi, Appl. Surf. Sci. **190**, 517 (2002).
[30] G. Henkelman, B. P. Uberuaga, and H. Jónsson, J. Chem. Phys. **113**, 9901 (2000).
[31] We have examined the adsorption of a N atom on surface O and Al atoms, and found that stable sites of the N atom are located above surface O atoms. However, the adsorption energy under nitridation conditions ($\sim$3.9 eV) is found to be quite large. It is thus unlikely that the adsorption of N adatoms on surfaces Al and O and desorption as NO molecules occur under nitridation conditions.
[32] M. Sano and M. Aoki, Jpn. J. Appl. Phys. **15**, 1943 (1976).
[33] T. Sasaki and S. Zembutsu, J. Appl. Phys. **61**, 2533 (1987).
[34] K. C. Pandey, Phys. Rev. Lett. **57**, 2287 (1986).